Accelerated publication

Advanced and reliable GaAs/AlGaAs ICP-DRIE etching for optoelectronic, microelectronic and microsystem applications

P.B. Vigneron[a], F. Joint[a,b], N. Isac[a], R. Colombelli[a], E. Herth[a,*]

[a] Centre de Nanosciences et de Nanotechnologies, CNRS UMR 9001, Univ. Paris-Sud, Université Paris-Saclay, C2N-Orsay, 91405 Orsay, Cedex, France
[b] Observatoire de Paris, Laboratory for Studies of Radiation and Matter in Astrophysics (LERMA),75014 Paris, France

ABSTRACT

We investigate the parameter optimization for micron-scale etching by Inductive Coupled Plasma - Deep Reactive Ion Etching (ICP-DRIE) of GaAs/AlGaAs semiconductor heterostructures. Although dry etching approaches have been reported in the literature using a broad variety of plasma etch tools, there is still need to meet the majority of microsystems dry etching requirements. The etch process family studied here, is dominated by the relative pressures of BCl_3 (Boron trichloride) and Cl_2 (Chlorine) gases. The influence of using a $BCl_3/Cl_2/Ar/N_2$ mixture at different pressures has been investigated: A small addition of N_2 (Nitrogen) is very effective inducing sidewall protection when using photoresist masks. The etch profile quality has been characterized as a function of the plasma process and of the etched feature sizes. The desired etch characteristics for GaAs/AlGaAs heterostructures can be achieved by controlling the various process parameters with good reliability, high selectivity, and – simultaneously – high etch rates and sidewall verticality. Etch rates from 1 to over $5.5\,\mu m/min$ have been obtained. The selectivity with optical photoresist varies from 2.3 to 16. The presented results can be valuable for a wide range of applications involving fabrication of micro-electro-mechanical-systems or Micro Optoelectronic Mechanical Systems.

1. Introduction

Current mainstream microelectronic and microsystem technology uses silicon as the substrate material [1–3]. III-V compound semiconductors, on the other hand, dominate of course optoelectronic applications [4–11]. However, III-V compound semiconductors suit high-performance applications even beyond optoelectronics, due to higher electron mobilities and peak velocities than silicon. As a consequence, there is growing interest for DRIE etching of III-V compound semiconductors and ICP reactors have been widely used in both manufacturing and research laboratories.

The BCl_3 and Cl_2-based chemistries are widely used in dry etching of III-V compound semiconductors. However, it is rare to use just Cl_2 or BCl_3 (or both together). Combinations with Ar or N_2 gases are generally employed [12–15], depending on the etched material system (GaAs, AlGaAs, GaP, GaSb and GaN) and also on the applications [16–23]. Sloped profiles may be necessary for some applications, such as a trenche, to guarantee adequate coverage during subsequent metal deposition. Vertical profiles (corresponding to an angle of 90 ± 2°) are essential for etching mirror facets for semiconductor lasers, or a cavity in the substrate for MEMS devices. In particular, III-V compound

semiconductors such as GaAs and AlGaAs are widely used for the microfabrication of sensor devices for applications in optoelectronics, optical wireless communications [24,25] and microsystems [26].

The aforementioned applications demand anisotropic etch profiles, as well as smooth sidewalls and surface morphology, and high etch rates and selectivity. Conventional reactive ion etching (RIE) is often used for the selective etch process of III-V compounds [23]. However, RIE processes rely on only one RF chuck (called platen or bias power), making it difficult to achieve good etch uniformity on large wafers (100 mm wafers are nowadays commonly used in III-V technology). Moreover, elevated RF platen bias are typically necessary to achieve vertical sidewalls. This also leads to high etch rates, but the physical impact of the ions on the III-V compounds and on the mask is increased too. The former one can cause damage to the device [27–29]. The latter one reduces the mask selectivity. One solution is to use an ICP-DRIE reactor where two power inputs are employed for the plasma. One is the platen power, similar to a RIE reactor. The other is the ICP source power. The latter one plays the crucial role of ionizing and generating the plasma. This technology provides almost independent control of ion density and ion energy, respectively. With optimized ICP conditions, typically a low RF chuck power and a high ICP source power, minimum
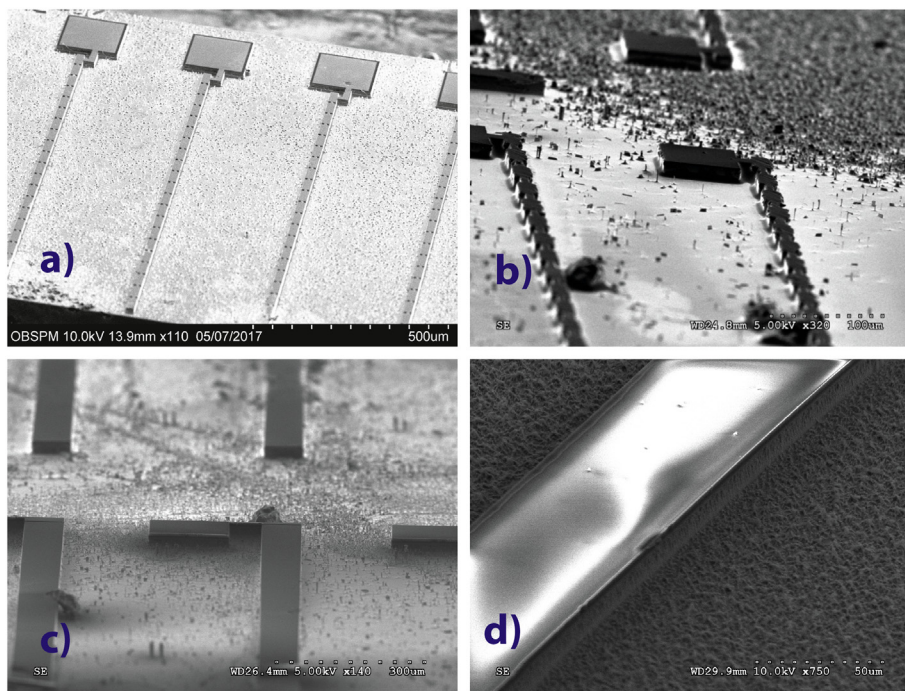
Fig. 1. SEM images of features etched into a GaAs wafer with micromasking effects apparent on the surface: a) with metal mask, b)-c) and d) with photoresist mask.
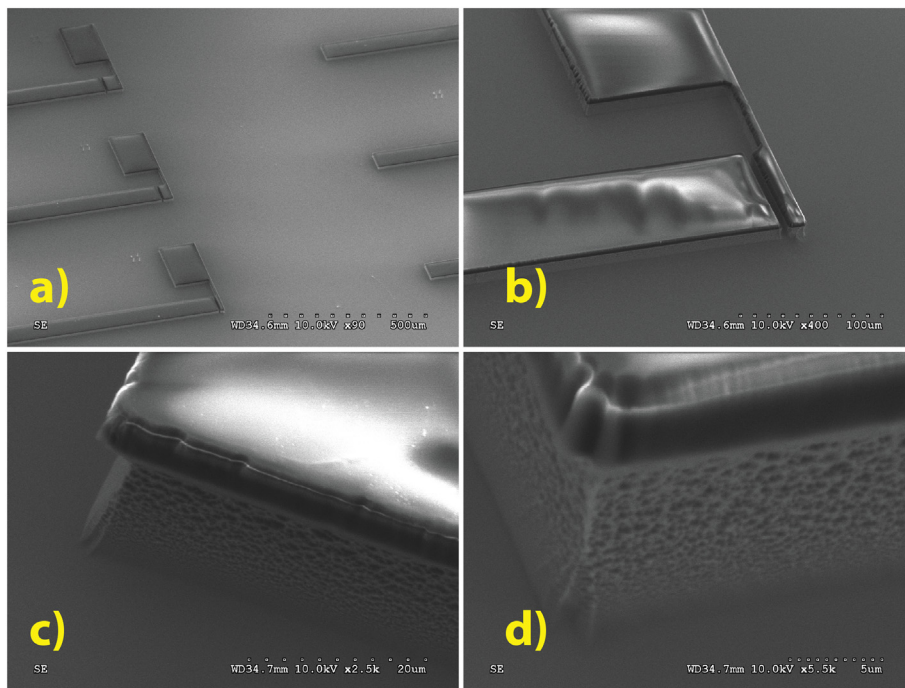

Fig. 2. SEM micrographs of a 6μm-thick etching of a GaAs wafer a-b)exhibiting a smooth floor, but c-d) rough sidewalls. This is typically found when using recipes R1-R4, that are Cl_2-based.

damage or damage-free etch with high etch rate and sidewalls can be obtained with III-V materials [15,30].

Several approaches to increase the etch selectivity have been developed. The use of gases promoting formation of polymer films on the surfaces was shown to favor the selectivity. In this article we show that a $BCl_3/Cl_2/N_2/Ar$ plasma chemistry can produce highly anisotropic etching of GaAs/AlGaAs heterostructures in combination with photoresist-based masks. Each ICP-DRIE etching parameter has an effect on the rate, anisotropy, surface roughness, and sidewall morphology. All of them must be carefully controlled for reliable device manufacturing.

Special attention has been paid to the problem of plasma-induced structural damages such as the micromasking and the sidewall roughness. Our objective is to optimize III-V compounds etching using a ICP-DRIE etcher. We have identified plasma conditions that provide not only an adequate surface chemistry but vertical and smooth sidewalls as well. The paper is organized as follows: section II describes the solution to overcome the micromasking phenomenon and to obtain a smooth surface using a photoresist mask (for low cost processing). Section III describes the ICP process for GaAs as a function of gas mixtures and pressures. In section IV, we investigate the sidewall quality and angle
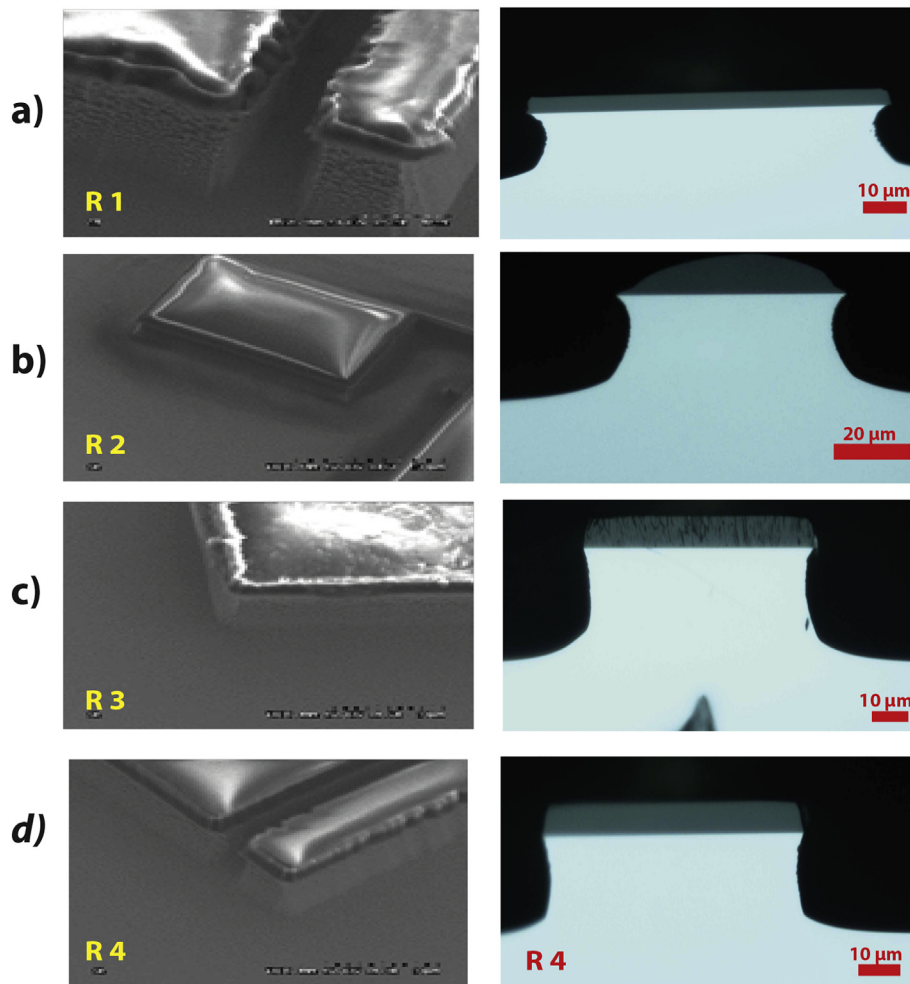
Fig. 3. SEM micrographs and corresponding optical photograph of features etched into GaAs with BCl$_3$/Cl$_2$/Ar. Typically found when using the recipes a) R1, b) R2 c) R3 and d)R4.

profile by exploring how the shape of the photoresist mask evolves during the ICP processes. We conclude with a discussion of these results and their potentiel applications.

2. Experiment

The experiments were performed in a STS (Surface Technology Systems) reactor, equipped with a maximum available power 900 W, 13.56 MHz RF coil generator. The gases employed in this study were BCl$_3$, Cl$_2$, Ar, N$_2$ and O$_2$. During all the experiments, the temperature of the electrode was fixed at 25˚C. A 5-min-long oxygen clean procedure was performed between each run to remove any polymer from the re-actor sidewalls, minimize contamination, and preserve process repeat-ability. The samples were loaded into the reactor by mounting them on an alumina carrier wafer with silicone grease to ensure good thermal contact. As part of the optimization of the etching parameters a mask design with different kinds of test structures (trenches and cavities) for measuring the process outcome was employed. In this investigation a surface inspection of the etch result was the best way to check the etch characteristics. All test samples were 1 cm × 1 cm pieces of bulk GaAs or GaAs /Al$_{0.15}$Ga$_{0.85}$As THz quantum cascade lasers [31].

We studied several different etch processes and their general char-acteristics were compared. Typical parameters from these processes are summarized in Table I, with an etching time set at 5 min for all the samples. Photoresist (AZ9260, 6μm-thick), was patterned with test geometries on GaAs wafers, or on GaAs /Al$_{0.15}$Ga$_{0.85}$As THz quantum

cascade heterostructures [31], and used as the mask material. The mask erosion was estimated by measuring its thickness pre- and post-etching for a fixed time. The mask selectivity was estimated by calculating the ratio of the semiconductor etch rate to photoresist etch rate. The samples were etched and studied using an optical microscope and a Scanning Electron Microscope (SEM). The latter one provides error on the measurement due to the pixel size of the image. The error bars on the depth and angle measurement, or on the etch rate and selectivity are plotted in all the figures.

3. Results

3.1. Micro-masking

Micro-masking occurs when material liberated during the etching is redeposited elsewhere on the sample and creates an undesirable addi-tional etch. It is most frequently encountered when a metal mask is used because of the physical sputtering of small metal particles, that are not volatile (as seen in Fig.1a). A photoresist mask may also induce polymer deposition on the etched sidewalls due to a reaction with the plasma and result in roughly etched surfaces due to micro-masking (as shown in Fig.1b, c and d). As a consequence, the micromasking phenomena can significantly reduce the etch rate. Fig. 2 shows SEM images of the samples after an etch with a Cl$_2$-based chemistry. The samples present very smooth bottom surfaces. However an undercut is also observed and the sidewalls are rough. As predicted for Cl$_2$-rich environments,

Table 1
Typical results from the different etch processes used in this study with coil power: platen power ratio fixed to 8:1 with an etching time set at 5 min for all samples.

Parameters					Results	
Recipe	Pa (mTorr)	BCl$_3$/Cl$_2$	Ar	N$_2$	Etch rate (μm/min)	Selectivity
1	10	4	0	0	3.64	6.67
2	10	2	0	0	3.6	6.5
3	10	2.5	0	0	2.38	4.3
4	10	4	5	0	2.38	4.43
5	10	2.5	5	0	2.13	3.73
6	10	6	5	0	2	4.12
7	10	6	0	0	2.37	2.71
8	10	8	0	0	2.1	4
9	10	6	5	2	3.84	5.95
10	10	6	5	2.5	4	7.22
11	10	6	5	3	4	6.2
12	10	3	5	3	2.5	2.3
13	10	12	5	3	1.6	3.9
14	10	20	5	3	1	2.85
15	10	20	5	3	1.8	4
16	5	20	5	3	1.14	2.5
17	10	20	5	3	1.8	4.22
18	20	20	5	3	2.36	5.2
19	25	20	5	3	3.6	11.26
20	30	20	5	3	3.7	12.33
21	30	20	5	5	5.56	16
22	20	20	5	5	4.1	10
23	10	20	0	3	1.92	3.35
24	20	20	10	3	2.8	8.9
25	20	20	20	3	3	8
26	20	20	30	3	2.5	7.28
27	20	20	50	3	2.23	6.42

Table 2
Dissociation enthalpy of BCl$_3$, Cl$_2$, N$_2$ and Ar used to enhance the etching rate of GaAs.

Parameters	BCl$_3$	Cl$_2$	N$_2$	Ar
Dissociation enthalpy (kcal mol^{-1})	110.7	58	226	363.73

GaAs and AlGaAs were chemically etched causing severe undercut as observed in Fig. 3, when using the recipes R1-R3. In BCl$_3$-rich environments instead, when using the recipe R4, GaAs and AlGaAs are in general slightly passivated and the undercut effect is reduced [32,33,34]. Note: BCl$_3$ may cause a problem because Boron-containing molecules can be deposited onto the wafer surface. By adding Ar in the BCl$_3$/Cl$_2$ mixture, it is possible to sputter these non volatile products away. With the Ar in the BCl$_3$/Cl$_2$ mixture, we obtained less under etching (see Table 1: R4, R24, R25, R26 and R27). The effects of the gas mixture on the etch characteristics of GaAs show that by increasing the Cl$_2$ flow rate, the etched surface becomes very smooth, but the etch profile is isotropic and the sidewalls are very rough. In the next section, the effect of plasma process parameters on the etch rate and the photoresist mask is studied.

3.2. High etch rate

The bulk micro-machining processes include wet etching, plasma (RIE or ICP DRIE) or both to realize microstructures. Because anisotropic wet etching often yields curved facets and rounded shapes, it is often not suitable for optoelectronic applications [35,36]. As a consequence, the ICP-DRIE etching remains a very good alternative since it does not introduce undercut or rounded edges, and it is highly flexible. Shallow etch depths and lower etch rates are desirable for pattern etching, whereas higher etch rates are preferred for very deep etching. Both these regimes can be attained with ICP-DRIE. A benchmark for the processes is an etch-rate greater or equal to 4 μm/min for a GaAs substrate.

Our objective is to develop a recipe with increased etch rate by facilitating the availability of chloride ions as a result of the reaction between BCl$_3$ and Cl$_2$. The addition of Ar or N$_2$ to the BCl$_3$/Cl$_2$ mixture affects the etch rates. In essence, adding Ar or N$_2$ can result in a different degree of dissociation of Cl$_2$. As shown in Table 2, the dissociation enthalpy of the used gases are different: a balance in terms of injected gas flow ratio and the power used is required. We investigated the introduction of N$_2$ to the BCl$_3$/Cl$_2$/ Ar mixture. It is important to note that adding only a very small amount of N$_2$ (2 or 5 sccm) already resulted in a sizeable increase of the GaAs etching rate, as shown in table I. From these results, it is also observed that the etch rate increases rapidly with increasing Cl$_2$ flow rate in the ratio BCl$_3$/Cl$_2$ due to the increase in the supply of reactive Cl$^+$ or Cl species at the sample surface. The change in etch rates as a function of the Cl$_2$ gas flow permits to infer if the process is reactant or diffusion limited. On the other hand, at a fixed Cl$_2$ flow, the etch rate increase with the BCl$_3$ flow is not as dramatic. This stems from the higher dissociation energy of BCl$_3$ molecules that leads to a smaller number of available Cl radicals for the reaction.

The optimum conditions for obtaining a higher etch rate were obtained at a high concentration of N$_2$ gas in the BCl$_3$/Cl$_2$/Ar mixture at 10 mTorr (see Table I: R9, R10 and R11) and at even higher operating pressures of 20–30 mTorr (see Table I: R20 and R21).

The addition of N$_2$ to the BCl$_3$/Cl$_2$:Ar (6:5) mixture increased the GaAs etch rate. For example, the etch rate of GaAs increased from 2 μm/min to 4 μm/min with the addition of 3 sccm of N$_2$. As shown in Fig. 4, the addition of N$_2$ also enhances the sidewall passivation preventing the isotropic undercut (typical of Cl$_2$-only based recipes) and produces a very anisotropic pattern transfer into the GaAs as well as into GaAs/AlGaAs heterostructures. We also observed that the etch rates of GaAs and of GaAs/AlGaAs heterostructures were not significantly different. As a matter of fact, the mechanisms for vertically etching bulk GaAs or GaAs/AlGaAs heterostructures are shown to be similar.

Fig. 4 shows the etch profiles as a function of operating pressure (Recipes R16-R18). Vertical profiles are obtained for pressures as high as 20 mTorr. The advantage of operating at higher pressure is to improve the selectivity with the photoresist mask. Nevertheless, the higher the pressure, the less smooth the sidewall surface is. However, the sidewall angle was always 9°. Note that maximum etch rates exceeding 3.8 μm/min (recipe 10) for 10 mTorr, and 5 μm/min (recipe 21) for higher pressure ranges from 20 to 30 mTorr are obtained in BCl3/Cl2/Ar/N2 with a good selectivity. These etching conditions suit the production in bulk GaAs and GaAs/AlGaAs heterostructures for MEMS, MOEMS and microlectronics applications. In the next section, a special attention is paid to the problem of plasma-induced structural damages such as the anisotropy and the sidewall roughness.

3.3. Smooth sidewall and angle

GaAs/AlGaAs-based waveguides are used for nonlinear optics applications, with advantages such as band-gap engineering flexibility and possibility to achieve broadband transparency throughout the telecommunication band. The performance of these waveguides is typically limited by the propagation losses, whose main source - in high-index contrast waveguides - is often the scattering due to the sidewall roughness and angle [37,38,39,40]. Positive-tone photoresists for device micro-fabrication were optimized to obtain a high resolution with excellent vertical profiles. Straight wall profiles achieve the best pattern fidelity. In fact, the mask erosion by the plasma ions mainly impacts the rounded or sloped edges of the photoresist mask. This results in an angled photoresist profile and - in case of deep etching - this angle is transferred to the etched pattern by gradual erosion of the photoresist at the mask edges. Furthermore, an increase in surface roughness on the top of the sidewalls (see Fig. 5.c) is in general observed.

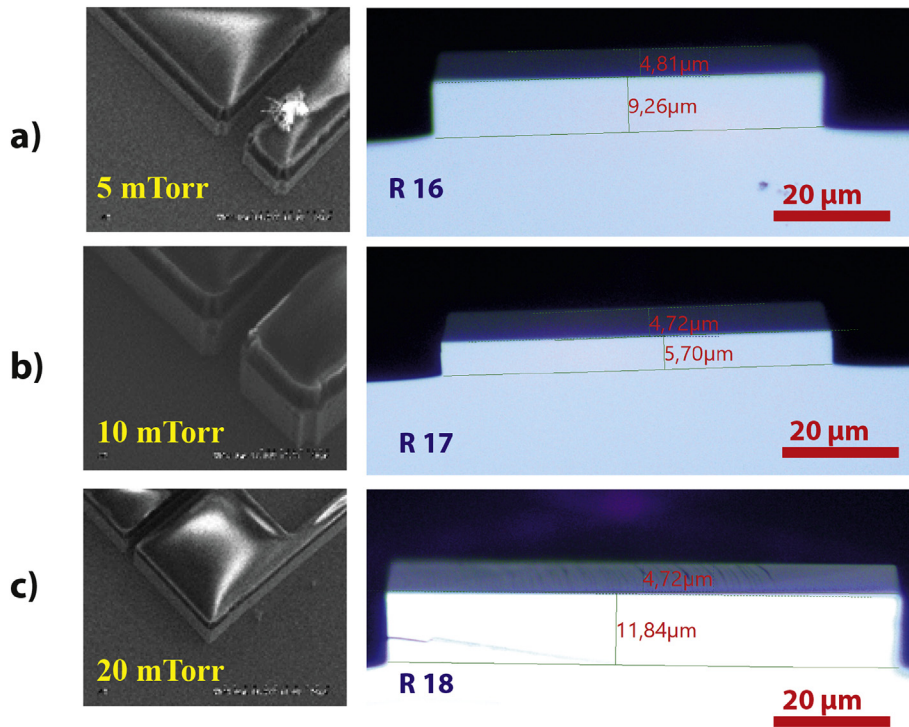Unfortunately, the major disadvantages of using a thick photoresist

Fig. 4. SEM micrographs and corresponding optical photograph of features etched into GaAs with $BCl_3/Cl_2/Ar$. Typically found when using recipes R16; R17 and R18.
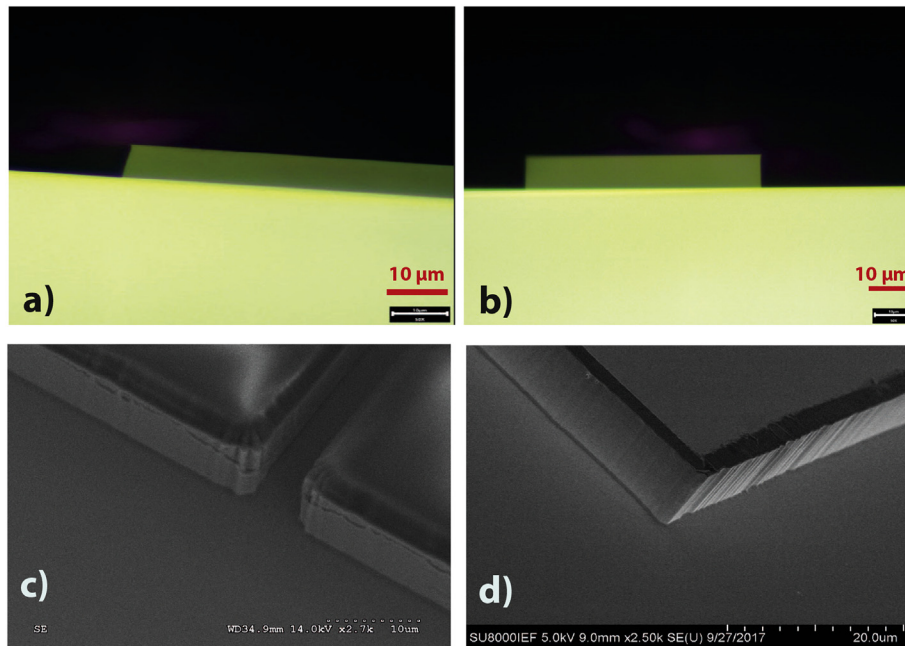

Fig. 5. (a,b): The AZ9260 photoresist profiles: the overcut profile (a) and the optimized vertical profile (b) (c,d): SEM images after etching a GaAs wafer sing a resist mask with overcut profille (c) and vertical profile (d).

are poor resolution and difficulty in obtaining straight wall profiles. The vertical striations on the sidewalls of the etched features appear to be related to edge roughness of the photoresist etch mask (see Fig. 4 at 5 mTorr and 10 mTorr).

As shown in Fig. 5, the micro-masking effect was completely absent when the sample was etched with N_2, under the same time and process conditions. The N_2 concentration in the plasma improves the smoothness of the etched profiles.

Increasing the BCl_3 flow reduces the etch rate, while increasing pressure enhances the selectivity, but the process becomes more

chemical thus leading to unwanted undercut features. In Fig. 6 we quantify this trend and we show - for a gas mixture ratio of BCl_3/Cl_2: 20 with N_2: 3 sccm - the experimental etch rate and selectivity as a function of operating pressure. The reason is that at lower pressure the mean free path of electrons, ions and neutrals is increased. The etch rate is reduced due to a more physical etching process, while at higher pressure the ion concentration on the GaAs surface enhances the chemical character of the etching. To be able to control the anisotropy of the process, the Ar concentration was adjusted by varying the relative flow rates. Despite the addition of Ar in the gas mixture BCl_3/Cl_2: 20,
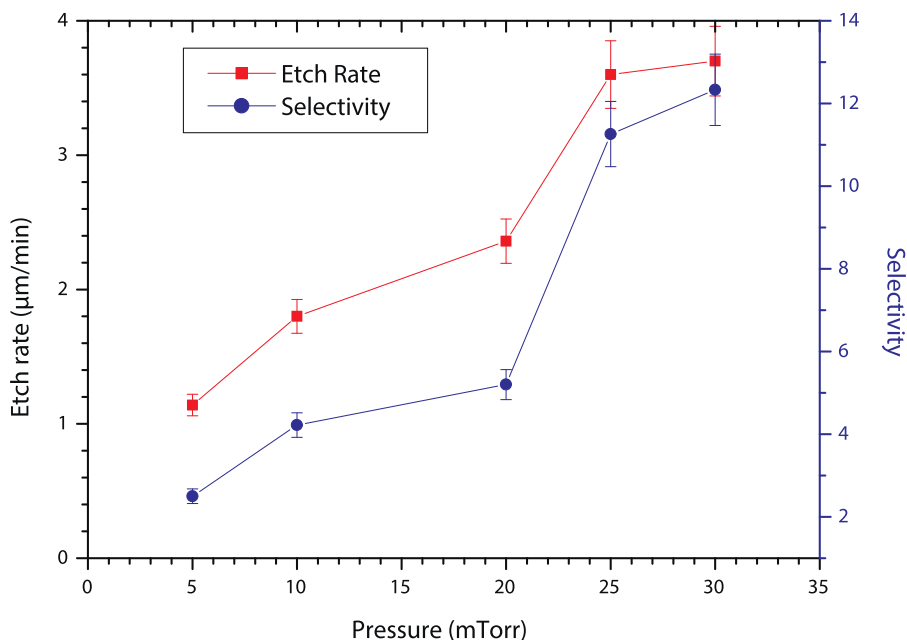
Fig. 6. GaAs etch rate and selectivity variation with pressure. The gas mixture is BCl_3/Cl_2:Ar 20:5 and N_2:3 sccm, (see Table 1: recipes 16 to 20).
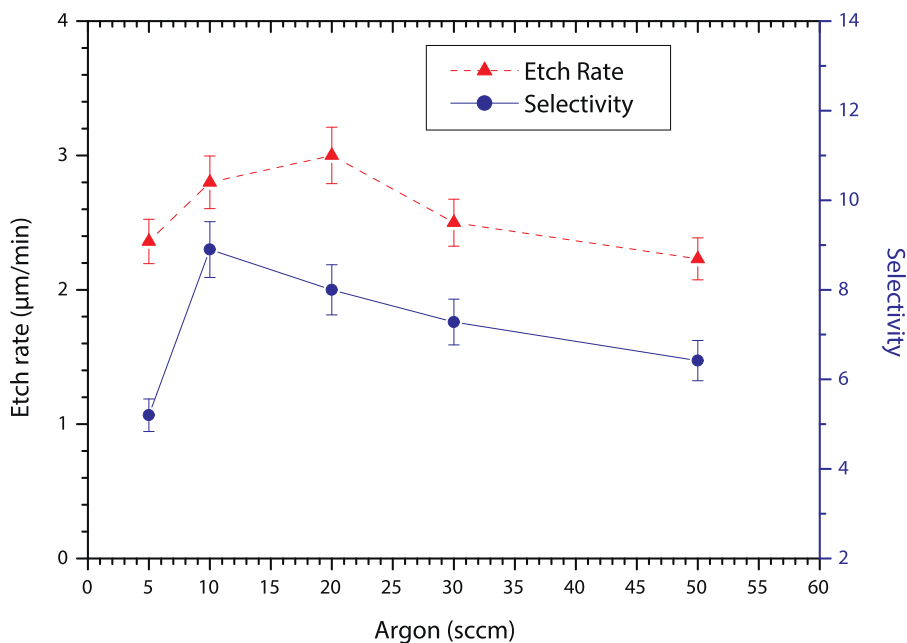

Fig. 7. GaAs etch rate and selectivity variation with argon. The gas mixture is BCl_3/Cl_2: 20 and N_2:3 sccm at 20 mTorr, (see Table I).

(see Table I: R4), some under etching with rough sidewalls was always observed and the slope was still found to be around 90°. On the other hand, by adding Ar in the gas mixture BCl_3/Cl_2: 20 with N_2: 3 sccm (see Table I), increasing the Ar gas flow from 5 to 50 sccm leads to an increase then a decrease of the etch rates as shown in Fig. 7. This trend in etch rate is attributed to a change from a chemically dominated reaction to a physically dominated one. This is further confirmed by the decreased selectivity with an increase in the Ar flow, due to the increased physical character of the etching. Compared to etching with BCl_3/Cl_2 or BCl_3/Cl_2/Ar, a mixture of BCl_3/Cl_2/Ar/N_2 yields smoother surfaces and vertical sidewalls without micro-masking effects. This is due to a balance of physical and chemical etching mechanisms. In contrast, we observe that micro-masking appears when we increase the N_2 proportion (with a threshold of 3 sccm.) and that the smooth surface

sidewall is not preserved at high pressure.

4. Discussion

Plasma etching is the result of a combination of isotropic chemical and anisotropic physical etchings. In ICP-DRIE reactor, the dominant etching mechanism for GaAs-based materials with a Cl_2/Ar chemistry is a chemical reaction, while with a BCl_3/Ar chemistry is physical sputtering [41]. An optimized recipe R15 has been developed. It yields anisotropic etching with moderate etch rate and very smooth surfaces. Compared to etching with only BCl_3/Cl_2 or BCl_3/Cl_2/Ar, a mixture of BCl_3/Cl_2/Ar/N_2 yields smoother surfaces and vertical sidewalls without a micro-masking effect.

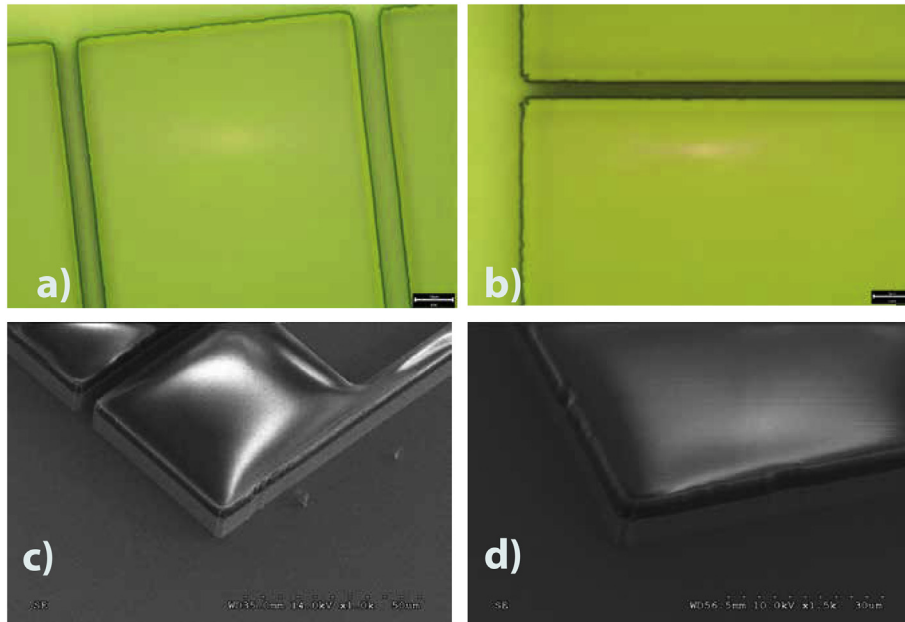Even with an optimized plasma etching process, the profile of the

Fig. 8. Ripple effects on GaAs etch rate: (a-b) optical view and (c-d) SEM view.
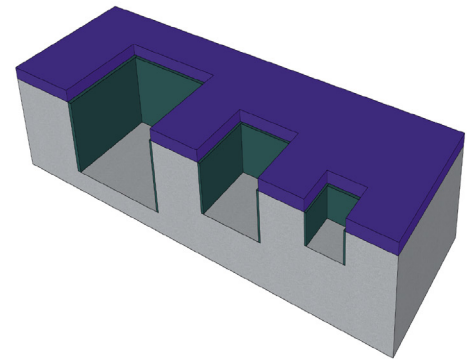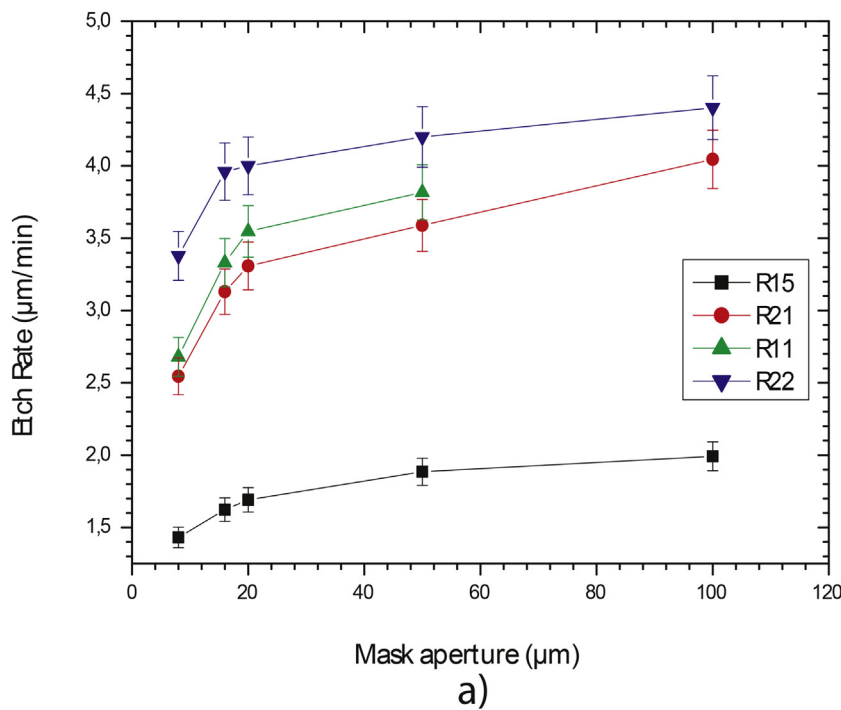

Fig. 9. ARDE effects: the GaAs etch rate is presented as a function of the mask aperture, a) for four different etching recipes (R11, R15, R21 and R22), b) illustration of ARDE.

photoresist sidewalls and the associated ripples are critical to many applications and do affect the quality of the etching. A vertical profile photoresist provides the best pattern fidelity, but it is relatively difficult to obtain. The presence of the ripples depends on the pattern and also on the conditions of the lithographic process. It often occurs, especially near concave corners. The resist wall profile and the ripple effect can be controlled by adjusting the photoresist, exposure dose, baking, developer strength, and development time (see Fig. 8).

One of the significant issues in this etch is the ARDE (Aspect Ratio Dependent Etch). In fact, the scaling of the etch rate with the feature dimension is an important issue in the fabrication of microelectronic and photonic devices. It requires a considerable effort to modify the etch processes each time changes in the design are made. As expected, as shown in Fig. 9, the GaAs etch rate depends on the mask opening size. In particular, the smallest mask opening was etched the slowest. Moreover, as shown in Fig. 10, the etch rate of GaAs and AlGaAs changes significantly as a function of the processing time. Nevertheless, the quality of the sidewalls is similar in both cases. Since, as highlighted before, the mechanisms for etching vertically bulk GaAs and GaAs/AlGaAs heterostructures are similar, the difference in selectivity between the two is purely a result of the difference in the etch rates of the semicondcutor material. The results reported in Fig.9a and Fig.10 are
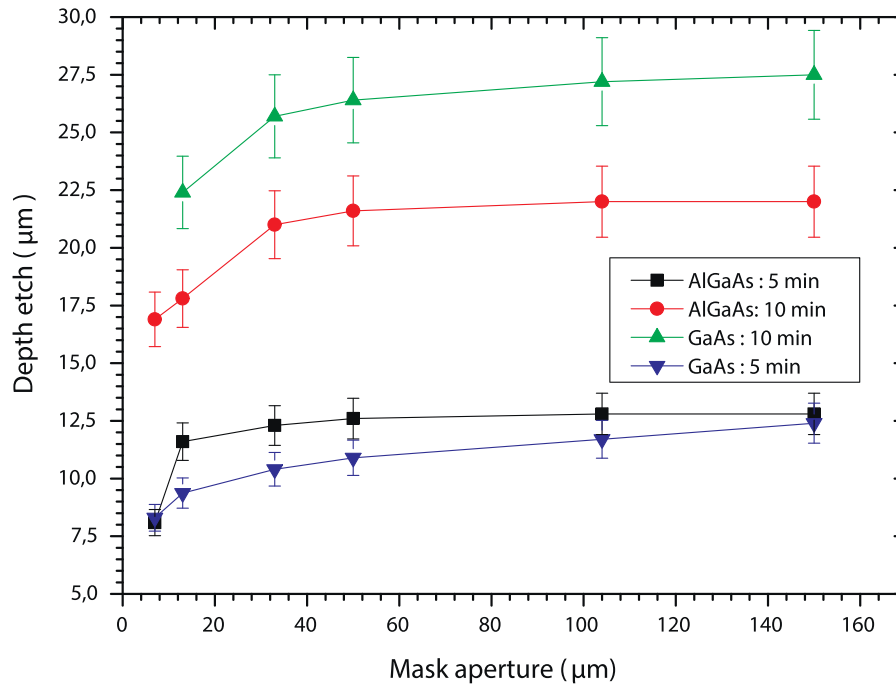
Fig. 10. Etch depth of GaAs and of a GaAs/AlGaAs heterostructure, as a function of the mask aperture size for two different etching times. (recipe R15).

Table 3
Comparison between our work and two representative results in the literature on the GaAs/AlGaAs etching using a ICP-DRIE reactor based on a BCl$_3$/Cl$_2$/N$_2$/Ar plasma chemistry.

Reference		Our work	[41]	[17]
Photoresist mask		AZ9260	SiO$_2$	AZ5214
Features	(μm)	2–100	0.08	3–10
Pressure chamber	(mTorr)	5–30	5	1
Coil Power/ Platen Power		8:1	10:1	8.5:1
BCl_3/Cl_2		≥2	1	1
Flow rate Ar	(sccm)	5–50	10	50
Flow rate N_2	(sccm)	2–5	n.c.	2–2.5
Chuck temperature	(°C)	25	20	10
Etch rate	(μm/min)	1–5.5	0.5–1.5	n.c.
Selectivity		2.5–16	20–100	n.c.
Depth	(μm)	5–30	2.6	n.c.

important because knowing how etch rates scale with design parameters accelerates the introduction of new designs into manufacturing while minimizing the cost of doing so.

In the literature, several studies of etching process parameters can be found using different etch masks (photoresist, insulator, metallic), size apertures, etch depths, and the etching time. We chose two significant examples (SiO2 and AZ5214 masks) and compared our results to them in Table III. Compared to the silicon oxide [41] and photoresist masks [17], our results suggest that it is possible to obtain a faster etching with improved selectivity.

In summary, this investigation proposes an etch process with high etch rate of GaAs/AlGaAs heterostructures, a good selectivity, anisotropic profiles, smooth surface morphology without any significant damage to the surface and sidewalls, using a thick photoresist mask which is a low cost organic polymer Table 3.

5. Conclusion

We have qualitatively and quantitatively investigated the link between various gas mixtures (and operating pressure) and micromasking, surface and sidewall smoothness, etch rates of GaAs/AlGaAs

semiconductor materials, and photoresist selectivity in a DRIE-ICP etch system. The choice of using photoresist masks provides a better flexibility and economical processing. Note that in an industrialization perspective, this development is compatible with Roll-to-Roll (R2R) technologies, thus allowing a massive production using only a single commercial ICP DRIE tool. The passivation layer induced by the addition of N$_2$ to the BCl$_3$/Cl$_2$/Ar plasma chemistry prevents lateral etching, thus producing smooth and nearly ideally vertical sidewalls. Nevertheless, beyond a N$_2$ threshold value of 3 sccm the enhanced passivation effect causes micromasking. A combination of different plasma parameters have been studied and the related ICP recipes can prove useful for optoelectronic, microelectronic and microsystem applications.

References

[1] V. Agache, B. Legrand, D. Collard, H. Fujita, L. Buchaillot, GHz silicon blade nano-electromechanical resonator featuring 20 nm gap lateral transducers 18th IEEE International Conference on Micro Electro Mechanical Systems, 2005. MEMS 2005, Vol. 1 (1) (2005) 121–124.
[2] J. Rutkowski, W. Fourcault, F. Bertrand, U. Rossini, S. Gétin, S. Le Calvez, T. Jager, E. Herth, C. Gorecki, M. Le Prado, J.M. Léger, S. Morales, Sensors Actuators A Phys. 216 (2014) 386–393.
[3] M. Faucher, B. Walter, A.S. Rollier, K. Seguini, B. Legrand, G. Couturier, J.P. Aime, C. Bernard, R. Boisgard, L. Buchaillot, Proposition of Atomic Force Probes Based on Silicon Ring-Resonators TRANSDUCERS 2007–2007 International Solid-State Sensors, Actuators and Microsystems Conference, (2007), pp. 1529–1532.
[4] G. Xu, R. Colombelli, S.P. Khanna, A. Belarouci, X. Letartre, L. Li, E.H. Linfield, A.G. Davies, H.E. Beere, D.A. Ritchie, Nat. Commun. 3 (952) (2012).
[5] F. Wang, H. Nong, T. Fobbe, V. Pistore, S. Houver, S. Markmann, N. Jukam, M. Amanti, C. Sirtori, S. Moumdji, R. Colombelli, L. Li, E. Linfield, G. Davies, J. Mangeney, J. Tignon, S. Dhillon, Laser & Photonics Reviews 11 n/a–n/a, (2017).
[6] C. Loyez, M. Fryziel, A. Boe, N. Rolland, P.A. Rolland, Microw. Opt. Technol. Lett. 42 (2004) 268–272 (ISSN 1098–2760).

[7] M. Heddebaut, F. Elbahhar, C. Loyez, N. Obeid, N. Rolland, A. Rivenq, J.M. Rouvaen, Transportation Research Part C: Emerging Technologies 18 (2010) 440–456.

[8] P. Lefevre, N. Haese, G. Lewandowski, C. Loyez, P.A. Rolland, E. Rogeaux, J.C. Sarkissian, A Full GaAs MMIC Phase-Locked Oscillator Using Sampling Phase Detector and a Sampling Frequency Detector, *2000 30th European Microwave Conference* pp 1–4, 2000.

[9] D. Bajoni, E. Semenova, A. Lemaître, S. Bouchoule, E. Wertz, P. Senellart, S. Barbay, R. Kuszelewicz, J. Bloch, Phys. Rev. Lett. 101 (266402) (2008).

[10] D. Bajoni, E. Semenova, A. Lemaître, S. Bouchoule, E. Wertz, P. Senellart, J. Bloch, Phys. Rev. B 77 (2008) 113303, https://doi.org/10.1103/PhysRevB.77.113303.

[11] D. Bajoni, P. Senellart, E. Wertz, I. Sagnes, A. Miard, A. Lemaître, J. Bloch, Phys. Rev. Lett. 100 (047401) (2008).

[12] G. Franz, A. Kelp, P. Messerer, J. Vac. Sci. Technol. A 18 (2000) 2053–2061.

[13] G. Franz, W. Hösler, R. Treichler, Journal of Vacuum Science & Technology B: Microelectronics and Nanometer Structures Processing, Measurement, and Phenomena 19 (2001) 415–419.

[14] I.K. Baek, W.T. Lim, J.W. Lee, M.H. Jeon, G. Cho, S.J. S And Pearton, Journal of Vacuum Science & Technology B: Microelectronics and Nanometer Structures Processing, Measurement, and Phenomena 21 (2003) 2487–2491.

[15] L. Jalabert, P. Dubreuil, F. Carcenac, S. Pinaud, L. Salvagnac, H. Granier, C. Fontaine, Microelectron. Eng. 85 (2008) 1173–1178.

[16] Y.Z. Juang, Y.K. Su, S.C. Shei, B.C. Fang, J. Vac. Sci. Technol. A 12 (1994) 75–82 (ISSN 0734-2101), 1520–8559.

[17] C. Constantine, Journal of Vacuum Science & Technology B: Microelectronics and Nanometer Structures 13 (1995) 2025 (ISSN 0734211X).

[18] J.W. Lee, J. Hong, E.S. Lambers, C.R. Abernathy, S.J. Pearton, W.S. Hobson, F. Ren, Plasma Chem. Plasma Process. 17 (1997) 155–167 (ISSN 0272-43241572–8986).

[19] R.J. Shul, G.B. McClellan, R.D. Briggs, D.J. Rieger, S.J. Pearton, C.R. Abernathy, J.W. Lee, C. Constantine, C. Barratt, J. Vac. Sci. Technol. A 15 (1997) 633–637 ISSN 0734-2101, 1520–8559.

[20] S. Agarwala, O. King, S. Horst, R. Wilson, D. Stone, M. Dagenais, Y.J. Chen, J. Vac. Sci. Technol. A 17 (1999) 52–55 ISSN 0734-2101, 1520–8559.

[21] M. Karlsson, F. Nikolajeff, Appl. Opt. 41 (902) (2002) 1539–4522.

[22] T. Maeda, J.W. Lee, R.J. Shul, J. Han, J. Hong, E.S. Lambers, S.J. Pearton, C.R. Abernathy, W.S. Hobson, Appl. Surf. Sci. 143 (1999) 174–182.

[23] S.J. Pearton, U.K. Chakrabarti, W.S. Hobson, A.P. Kinsella, J. Vac. Sci. Technol. B 8 (1990) 607–617 (ISSN 0734-211X).

[24] E. Herth, N. Rolland, T. Lasri, IEEE Antennas and Wireless Propagation Letters 9 (2010) 934–937.

[25] E. Herth, S. Seok, N. Rolland, T. Lasri, Sensors Actuators A Phys. 173 (2012) 238–243.

[26] V. Lacour, E. Herth, F. Lardet-Vieudrin, J.J. Dubowski, T. Leblois, Procedia Engineering 120 (2015) 721–726.

[27] S.J. Pearton, U.K. Chakrabarti, W.S. Hobson, J. Appl. Phys. 66 (1989) 2061–2064.

[28] S.W. Pang, G.A. Lincoln, R.W. McClelland, P.D. Degraff, M.W. Geis, W.J. Piacentini, J. Vac. Sci. Technol. B 1 (1983) 1334–1337 (ISSN 0734-211X).

[29] G. Franz, J. Vac. Sci. Technol. A 19 (2001) 762–772.

[30] A. Larrue, D. Belharet, P. Dubreuil, S. Bonnefont, O. Gauthier-Lafaye, A. Monmayrant, F. Lozes-Dupuy, S. Moumdji, Journal of Vacuum Science & Technology B, Nanotechnology and Microelectronics 29 (2011) 021006.

[31] G. Xu, L. Li, N. Isac, Y. Halioua, A. Giles Davies, E.H. Linfield, R. Colombelli, Appl. Phys. Lett. 104 (2014) 091112.

[32] K.A. Atlasov, P. Gallo, A. Rudra, B. Dwir, E. Kapon, J. Vac. Sci. Technol. B 27 (2009) L21.

[33] Y. Chen, B.S. Ooi, G.I. Ng, C.L. Tan, Y.C. Chan, Dry plasma etching of GaAs vias using BCl₃/Ar and Cl₂/Ar plasmas *Design, Fabrication, and Characterization of Photonic Devices*, International Society for Optics and Photonics, 3896 1999, pp. 199–207.

[34] G.T. Edwards, A. Sobiesierski, D.I. Westwood, P.M. Smowton, Semicond. Sci. Technol. 22 (2007) 1010.

[35] Z.L. Zhang, N.C. MacDonald, J. Microelectromech. Syst. 2 (1993) 66–73.

[36] A. Bienaime, C. Elie-Caille, T. Leblois, J. Nanosci. Nanotechnol. 12 (2012) 6855–6863.

[37] J.S. Aitchison, D.C. Hutchings, J.U. Kang, G.I. Stegeman, A. Villeneuve, IEEE J. Quantum Electron. 33 (1997) 341–348.

[38] H.E.G. Arnot, H.P. Zappe, J.E. Epler, B. Graf, R. Widmer, H.W. Lehmann, Electron. Lett. 29 (1993) 1131–1133.

[39] J. Shin, Y.C. Chang, N. Dagli, Opt. Express 17 (2009) 3390–3395.

[40] G.A. Porkolab, P. Apiratikul, B. Wang, S.H. Guo, C.J.K. Richardson, Opt. Express 22 (2014) 7733–7743.

[41] M. Volatier, D. Duchesne, R. Morandotti, R. Arès, V. Aimez, Nanotechnology 21 (2010) 134,014.